

An Efficient Element-Free Galerkin Method Based on Adaptive TR-AB2 Scheme for Transient Heat Conduction Problems

Shuyi Xiang and Xiaohua Zhang

Abstract—Meshless methods have numerous advantages over mesh-based approaches, but their high computational cost has significantly hindered their progress, particularly for time-dependent problems. In this study, we propose a time-adaptive meshless approach aimed at improving the computational efficiency of the method for addressing time-dependent issues. Specifically, we use the element-free Galerkin (EFG) method for spatial discretization, and the trapezoidal rule (TR) with adaptive time stepping for time integration. Additionally, we incorporate the explicit second-order Adams-Bashforth (AB2) method to control the error. The adaptive control of the time step effectively resolves issues related to non-convergence and low computational efficiency caused by inappropriate selection of the time step. To validate the efficacy and accuracy of the algorithm, we provide several numerical examples. The numerical results demonstrate that the EFG method combined with TR-AB2 method (EFG-TR-AB2) exhibits significant potential in solving two-dimensional transient heat conduction problems, which can maintain computational accuracy and improve computational efficiency.

Index Terms—time-adaptive, element-free Galerkin, trapezoidal rule, second-order Adams-Bashforth, transient heat conduction

I. INTRODUCTION

HEAT transfer [1] is one of the most common physical phenomena in nature, playing a crucial role in various energy conversion methods and the production process of objects, including heat conduction, convection, and radiation. Specifically, the transient heat conduction problem aims to investigate the heat transfer generated by the change of heat energy in the temporal domain. In recent decades, it has attracted attention because of its importance in engineering applications, including nanomaterials, energy systems, and thermoelectric devices.

Therefore, seeking an analytical solution for the transient heat conduction issue holds significant engineering and theoretical significance. However, analytical solutions are difficult to solve except few simplified cases because of the complexity of the problem, including factors such as boundary conditions and geometrical shapes. As a result, numerical solutions are commonly studied. Numerical methods used to solve such problems can be broadly categorized into two types, one is mesh-based method, including finite element method (FEM) [2], boundary element method [3], and so

on, and the other is meshless method [4]. In these mesh-based methods, mesh generation can be both time-consuming and tedious. In addition, in the case where the geometry of the solution region is complex, distorted meshes are often inevitably generated, further deteriorating the performance of the method. Therefore, meshless methods have gained wide attention as novel approaches to overcome these challenges. In the meshless method, discrete nodes are used to replace mesh elements, and shape function (SF) can be constructed by defining only the nodes, which avoids complex mesh generation.

Meshless methods can be categorized into two groups: meshless methods based on collocation strong form and meshless methods based on Galerkin weak form [5]. The representative collocation meshless methods are radial basis collocation method (RBCM) [6], reproducing kernel collocation method (RKCM) [7], etc. However, the meshless method based on collocation strong form is less accurate and unstable than the meshless method based on Galerkin weak form. The typical Galerkin meshless methods are EFG method [8], reproducing kernel particle method (RKPM) [9], etc. Among them, the EFG method has greatly advanced the development of the meshless method due to its high calculation accuracy and rapid convergence speed.

In recent decades, the study of meshless methods has been widely concerned on heat conduction problems. Take EFG method as an example. The nonlinear transient heat conduction problem of material properties varying with temperature is studied by Singh et al. [10] using EFG method. Sharma [11] used EFG method to study transient heat conduction problems of viscous fluid flow. Cheng et al. [12] combined the dimension splitting (DS) method with the improved complex variable EFG method to solve transient heat conduction problems. Although EFG method is widely employed in transient heat conduction research, its computational time is comparatively higher than that of the mesh-based method due to variations in shape functions (SFs) and their derivatives at different points. In addition, the process of calculating the SF involves the inversion of the matrix and the multiplication between multiple matrices, which are more complicated. Compared with the mesh-based algorithm, the computational efficiency is not competitive, which hinders the development of the EFG method. Therefore, it is necessary to find some ways to enhance the computational efficiency of EFG method, especially for time-dependent problems.

To solve the above problems, many scholars have made corresponding efforts. zhang et al. [13] proposed an improved EFG (IEFG) method to study transient heat conduction problems by combining the EFG method with the improved

Manuscript received May 10, 2023; revised September 27, 2023.

Shuyi Xiang is a graduate student of College of Science, China Three Gorges University, Yichang 443002, China, (e-mail: dreamingxw@163.com).

Xiaohua Zhang is an associate professor of School of Mathematics, Yunnan Normal University, Kunming 650500, China, (corresponding author, e-mail: zhangxiaohua@ynnu.edu.cn).

moving least squares (MLS) approximation. While maintaining the same accuracy, the IIEFG method exhibits higher computational efficiency compared to the EFG method. Sun et al. proposed an improved interpolating EFG (IIEFG) method [14] by combining the EFG method with the improved interpolation MLS (IIMLS) method [15]. The IIEFG method can directly apply the displacement boundary conditions, which saves a lot of calculation time than the EFG method. Wang et al. proposed a dimension-splitting MLS (DS-MLS) method by coupling DS with MLS method [16], and then, DS-MLS method is coupled with the EFG method to propose an improved EFG method (IEFGM) [17]. The IEFGM method offers improved calculation accuracy and reduced computation time for some two-dimensional potential problems in irregular regions. These methods improve the computational efficiency to some extent, but the effect is not very significant for long time simulation problems.

To tackle this issue, we find that we can start with another method, namely adaptive control time step. In numerical calculation, to enhance calculation accuracy, the smaller time step is usually set, which will lead to high calculation costs. If the large time step is set to save calculation cost, it may lead to the divergence of the calculation results or even the sudden interruption of the calculation. Time adaptation can effectively solve the issue related to non-convergence and low computational efficiency caused by inappropriate selection of time step, which has been proved in mesh-based methods. Bosco et al. [18] proposed an adaptive FEM approach for solving the evolution convection-diffusion problem by combining FEM with the TR-AB2 [19] method, and it is verified through numerical examples the effectiveness of this approach. Gee et al. [20] proposed an adaptive time-stepping fluid-structure interaction (FSI) solvers. Numerical examples show that this method can achieve the required accuracy control and save computational costs. Wang et al. [21] proposed an adaptive time-stepping semi-Lagrangian method aimed at obtaining higher simulation accuracy and solving advection problems. However, there are few reports on the combination of meshless method and time adaptive method thus far. In this study, we propose the EFG-TR-AB2 method, which combines the EFG method with the renowned TR-AB2 method. The TR-AB2 method is absolutely stable. To assess the effectiveness of the EFG-TR-AB2 method, we compare it with the EFG method combined with the Crank-Nicolson (EFG-CN) method. The EFG-CN method utilizes spatial discretization through the EFG method and time integration using the Crank-Nicolson (CN) method. The CN method usually adopts a fixed time step and is unconditionally stable.

An outline of the paper is as follows. In Section II, the governing equation of transient heat conduction is provided. In Section III, the EFG method is used for spatial discretization. In Section IV, the TR-AB2 method is used for time discretization. In Section V, we provide several numerical examples and summarized in Section VI.

II. MODEL PROBLEM

The governing equations and initial conditions of two-dimensional transient heat conduction can be generally expressed as [22]

$$\rho c_p \frac{\partial T}{\partial t} = \frac{\partial}{\partial x} (k_x \frac{\partial T}{\partial x}) + \frac{\partial}{\partial y} (k_y \frac{\partial T}{\partial y}), \quad \text{in } \Omega, \quad (1)$$

$$T(x, y, 0) = T_0, \quad \text{in } \Omega, \quad (2)$$

and subject to the conditions on the boundary $\Gamma = \Gamma_b \cup \Gamma_q$

$$T = T_b, \quad \text{on } \Gamma_b, \quad (3)$$

$$k_x \frac{\partial T}{\partial x} n_x + k_y \frac{\partial T}{\partial y} n_y = q, \quad \text{on } \Gamma_q, \quad (4)$$

where T is temperature, ρ is material density, c_p is material specific heat, k_x, k_y is the thermal conductivity in x and y directions, respectively; T_0 is the initial temperature, $\mathbf{n} = (n_x, n_y)$ is the outward unit normal to Γ , T_b and q are the prescribed temperature and heat fluxes on Dirichlet boundaries Γ_b and Neumann boundaries Γ_q , respectively.

III. NUMERICAL IMPLEMENTATION OF EFG METHOD

To obtain the approximate solution of two-dimensional transient heat conduction equation, the discrete system equation of the problem needs to be established. Initially, we write the Eq. (1) in weak form.

Let $V = \{v \in H^1(\Omega) : v|_{\Gamma_b} = T_b\}$, where $H^1(\Omega)$ is Hilbert space [23]. Multiplying a test function $w \in V_0 = \{v \in H^1(\Omega) : v|_{\Gamma_b} = 0\}$ with Eq. (1), and using Green's formula for integration by parts, we can derive the weak form of Eq. (1): find $T \in V$ such that

$$\begin{aligned} & \int_{\Omega} \rho c_p w \frac{\partial T}{\partial t} d\Omega + \int_{\Omega} (k_x \frac{\partial w}{\partial x} \frac{\partial T}{\partial x} + k_y \frac{\partial w}{\partial y} \frac{\partial T}{\partial y}) d\Omega \\ & = \int_{\Gamma_q} w q d\Gamma, \quad \forall w \in V_0. \end{aligned} \quad (5)$$

Let V_h represent a finite-dimensional subspace of infinite-dimensional space V , $V_{h,0} = V_h \cap V_0$, and derive the discrete system equation, it is necessary to find the meshless approximation function $T_h \in V_h$

$$\begin{aligned} & \int_{\Omega} \rho c_p w_h \frac{\partial T_h}{\partial t} d\Omega + \int_{\Omega} (k_x \frac{\partial w_h}{\partial x} \frac{\partial T_h}{\partial x} + k_y \frac{\partial w_h}{\partial y} \frac{\partial T_h}{\partial y}) d\Omega \\ & = \int_{\Gamma_q} w_h q d\Gamma, \quad \forall w_h \in V_{h,0}. \end{aligned} \quad (6)$$

In different meshless methods, approximate function method is different. EFG method is usually the MLS method.

A. MLS Approximation

Firstly, the MLS approximation function $T_h(\mathbf{x})$ of the unknown function $T(\mathbf{x})$ on the field Ω can be expressed as [24]

$$T_h(\mathbf{x}) = \sum_{i=1}^m Q_i(\mathbf{x}) \xi_i(\mathbf{x}) = \mathbf{Q}^T(\mathbf{x}) \boldsymbol{\xi}(\mathbf{x}), \quad (7)$$

where $\boldsymbol{\xi}(\mathbf{x}) = \{\xi_1(\mathbf{x}), \xi_2(\mathbf{x}), \dots, \xi_m(\mathbf{x})\}^T$ in Eq. (7) is an unknown coefficient vector.

For two-dimensional problems, in order to facilitate the calculation, the linear basis function is generally chosen as basis function, and its form is

$$Q(x) = [1, x, y]^T.$$

$\xi(x)$ is obtained by weighted least squares fitting, that is, for any point x , the choice of $\xi(x)$ always takes the minimum value of the following discrete L_2 norm

$$J = \sum_{i=1}^n \omega(x - x_i) [Q^T(x_i)\xi(x) - T_i]^2. \quad (8)$$

There are multiple choices for weight functions $\omega(x - x_i)$, including exponential function, Gauss function, cubic spline function (CSF) [25], etc. In this paper, CSF is selected

$$\omega(x - x_i) = \omega_i(\gamma) = \begin{cases} \frac{2}{3} - 4\gamma^2 + 4\gamma^3, & \gamma \leq \frac{1}{2}, \\ \frac{4}{3} - 4\gamma + 4\gamma^2 - \frac{4\gamma^3}{3}, & \frac{1}{2} < \gamma \leq 1, \\ 0, & \gamma > 1, \end{cases} \quad (9)$$

where $\gamma = \frac{\|x - x_i\|}{\rho_i}$, $\|x - x_i\|$ represents the distance between x and x_i , $\rho_i = \alpha d_i$ is the influence radius of node x_i , d_i represents the distance between adjacent nodes near interpolation point, and α is the influence factor.

J minimizes with respect to $\xi(x)$

$$\frac{\partial J}{\partial \xi} = A(x)\xi(x) - B(x)T = 0, \quad (10)$$

where

$$A(x) = \sum_{i=1}^n \omega_i(x)Q(x_i)Q^T(x_i), \quad (11)$$

$$B(x) = [\omega_1(x)Q(x_1), \omega_2(x)Q(x_2), \dots, \omega_n(x)Q(x_n)]. \quad (12)$$

By Eq. (10), we can get

$$\xi(x) = A^{-1}(x)B(x)T. \quad (13)$$

Substituting Eq. (13) into Eq. (7), it can be obtained

$$\begin{aligned} T_h(x) &= Q^T(x)\xi(x) \\ &= Q^T(x)A^{-1}(x)B(x)T = \Phi^T(x)T, \end{aligned} \quad (14)$$

where $\Phi(x)$ is the MLS shape function (MLS-SF)

$$\Phi^T(x) = Q^T(x)A^{-1}(x)B(x). \quad (15)$$

In general, the SF calculated using the MLS method cannot satisfy the Kronecker Delta function property (KDFP), which means that the Dirichlet boundary condition cannot be directly applied. Currently, numerous scholars have proposed some methods to overcome this shortcoming. For example, Lagrange multiplier method [26] and penalty function method [27], etc. However, these methods either increase the computational workload, or the choice of parameters is not very convenient. This paper adopts the convex polygon influence domain technology proposed by Zhang et al [28]. This method extends the rectangular influence domain to any convex polygon shape and for any convex polygonal node influence domain, while the influence factor approaches 1, the value of the MLS-SF at the node is almost equal to 1. This implies that as the dimensionless size is close to 1, the

MLS-SF at the node nearly has the KDFP. In this way, the EFG method can impose boundary conditions as simple as the FEM. The specific introduction of this method can be referred to [28].

First-order partial derivatives of approximate functions for x and y are involved in the numerical calculation, which can usually be transformed into the calculation of the first-order partial derivatives of SF Φ for x and y . To avoid the inverse multiplication of multiple matrices and reduce the workload, Eq. (15) is reformulated as [29]

$$\Phi^T(x) = \Theta^T(x)B(x), \quad (16)$$

that is to say

$$\Theta^T(x) = Q^T(x)A^{-1}(x). \quad (17)$$

A is a symmetric matrix, so $\Theta(x)$ can be obtained by Eq. (17)

$$A\Theta = Q. \quad (18)$$

The first-order partial derivatives of Θ for x and y can be calculated by

$$A \frac{\partial \Theta}{\partial x} = \frac{\partial Q}{\partial x} - \frac{\partial A}{\partial x} \Theta, \quad (19)$$

$$A \frac{\partial \Theta}{\partial y} = \frac{\partial Q}{\partial y} - \frac{\partial A}{\partial y} \Theta, \quad (20)$$

then the first-order partial derivatives of Φ for x and y can be calculated by

$$\frac{\partial \Phi^T}{\partial x} = \frac{\partial \Theta^T}{\partial x} B + \Theta^T \frac{\partial B}{\partial x}, \quad (21)$$

$$\frac{\partial \Phi^T}{\partial y} = \frac{\partial \Theta^T}{\partial y} B + \Theta^T \frac{\partial B}{\partial y}. \quad (22)$$

B. The Formula of EFG Method

Substituting Eqs. (14), (21) and (22) into Eq. (6), a semi-discrete ordinary differential equation (ODE) is obtained

$$M\dot{T} + KT = F, \quad (23)$$

where T is the vector of the temperature of the unknown node, \dot{T} is the first derivative of T for time, and the heat capacitance matrix M , the heat conductance matrix K and the load vector F are as follows:

$$M_{ij} = \int_{\Omega} \rho c_p \phi_i(x) \phi_j(x) d\Omega, \quad (24)$$

$$K_{ij} = \int_{\Omega} (k_x \frac{\partial \phi_i}{\partial x} \frac{\partial \phi_j}{\partial x} + k_y \frac{\partial \phi_i}{\partial y} \frac{\partial \phi_j}{\partial y}) d\Omega, \quad (25)$$

$$F_i = \int_{\Gamma_q} q \phi_i(x) d\Gamma. \quad (26)$$

IV. TIME DISCRETIZATION

There are many methods available for solving ODE, including the forward Euler method, the backward Euler method, the CN method, etc. Generally speaking, these methods employ fixed step sizes which require very small time steps to ensure accuracy. However, when there is minimal change in solution behavior, utilizing small time steps becomes inefficient. To enhance the efficiency of meshless computing, we can control the time step adaptively. In this paper, the TR-AB2 method is used to integrate the Eq. (23). This algorithm consists of three main components: time integration, time step selection method, and stabilization of the integrator. The following is a detailed explanation.

A. Time Integration

Rewrite Eq. (23) as

$$\dot{\mathbf{T}} = \mathbf{M}^{-1}(\mathbf{F} - \mathbf{K}\mathbf{T}), \quad (27)$$

from the trapezoidal rule, we can get:

$$\begin{aligned} \mathbf{T}_{n+1} &= \mathbf{T}_n + \frac{1}{2}\Delta t_n(\dot{\mathbf{T}}_{n+1} + \dot{\mathbf{T}}_n) \\ &= \mathbf{T}_n + \mathbf{M}^{-1}(\mathbf{F} - \frac{1}{2}\mathbf{K}(\mathbf{T}_{n+1} + \mathbf{T}_n)). \end{aligned} \quad (28)$$

It should be noted that because there is often a rounding error accumulation, it will lead to the generation of time step asymptotes, and prevent them from increasing at the desired speed. That is to say, the implementation of this linear multistep in the adaptive algorithm is likely to have a “stall” tendency. Moreover, Eq. (28) requires matrix inversion, which can be time-consuming. To minimize the potential rounding instability and enhance the computational efficiency, the TR-AB2 method updates the vector scaled by time step. To be specific, given the \mathbf{T}_n , $\dot{\mathbf{T}}_n$ and $\ddot{\mathbf{T}}_n$, $\tilde{\mathbf{T}}_n$ can be calculated first by [19]

$$(\mathbf{M} + \frac{1}{2}\Delta t_n\mathbf{K})\tilde{\mathbf{T}}_n = \mathbf{M}\dot{\mathbf{T}}_n - \mathbf{K}\mathbf{T}_n + \mathbf{F}, \quad (29)$$

\mathbf{M} , \mathbf{K} and \mathbf{F} can be obtained from Eqs. (24), (25) and (26).

Then use the obtained $\tilde{\mathbf{T}}_n$ to update the TR solution vector \mathbf{T}_{n+1} . Additionally, calculate the time derivative $\dot{\mathbf{T}}_{n+1}$ required for the next operation

$$\mathbf{T}_{n+1} = \frac{1}{2}\Delta t_n\tilde{\mathbf{T}}_n + \mathbf{T}_n, \quad (30)$$

$$\dot{\mathbf{T}}_{n+1} = \tilde{\mathbf{T}}_n - \dot{\mathbf{T}}_n. \quad (31)$$

The adaptive time step is implemented through control of the local truncation error (LTE) related to each time step. The TR-AB2 method uses the explicit AB2 method to estimate the LTE. Firstly, the AB2 method updates $\tilde{\mathbf{T}}_n$ by

$$\tilde{\mathbf{T}}_n = \dot{\mathbf{T}}_n + \frac{1}{2}(\dot{\mathbf{T}}_{n+1} - \dot{\mathbf{T}}_n), \quad (32)$$

then use $\tilde{\mathbf{T}}_n$ to calculate LTE [30]:

$$\mathbf{d}_n = \frac{\Delta t_n}{3(1 + \Delta t_{n-1}/\Delta t_n)}(\frac{1}{2}\tilde{\mathbf{T}}_n - \tilde{\mathbf{T}}_n). \quad (33)$$

In program implementation, because the AB2 can not self-start, first few steps should be guided by a one-step method,

and then turn to the multi-step method. Therefore, we first calculate $\dot{\mathbf{T}}_0 = \mathbf{M}^{-1}(\mathbf{F} - \mathbf{K}\mathbf{T}_0)$ through Eq. (23), take $\Delta t_1 = \Delta t_0$ as a small value (for example 10^{-9}), and use Eqs. (29) and (31) to calculate $\dot{\mathbf{T}}_1$. Then turn on the error control and Δt change at the third time step.

B. Time Step Selection

Because of the need to achieve an adaptive time step by controlling the LTE associated with each time step, we have estimated the LTE in the previous section, and then need to predict the LTE at the next step. The ratio of the continuous LTE $\frac{\|\mathbf{d}_{n+1}\|}{\|\mathbf{d}_n\|}$ is proportional to the cube of the ratio of the continuous time steps $(\frac{\Delta t_{n+1}}{\Delta t_n})^3$. Consequently, though setting a user-specified tolerance (this article selects $\epsilon = 10^{-4}$) can control the next LTE $\|\mathbf{d}_{n+1}\| \leq \epsilon$ [31]. Then the next time step can be selected, that is, the time step selection heuristic is obtained:

$$\Delta t_{n+1} = \Delta t_n(\epsilon/\|\mathbf{d}_{n+1}\|)^{\frac{1}{3}}, \quad (34)$$

where $\|\cdot\|$ is a properly defined vector norm. The choice of this norm affects the required LTE tolerance value to achieve a certain level of global accuracy. However, it is anticipated that it will not have a substantial influence on the qualitative behavior of the adaptive time-stepping algorithm. This paper refers to the reference [19], using the L_2 norm

$$\|\mathbf{d}_n\| = (\mathbf{d}_n^T \mathbf{M} \mathbf{d}_n)^{1/2}. \quad (35)$$

C. Stabilization of the Integrator

TR is highly recommended because it has A-stability and optimal accuracy [32], and adaptive time steps that accommodate error control [33]. However, the TR scheme is also known to suffer from “ringing” instability. This ringing effect occurs from the absence of L-stability in the TR method, resulting in a ringing effect when the time step is too large. But this, in turn, can cause the adaptive time step algorithm to stall, meaning that even if the physical conditions allow, the time step cannot continue to grow and remains smaller than required. As a result, computing efficiency cannot be effectively improved. To counteract the ringing effect that TR is prone to, that is, to suppress oscillations, Gresho et al. [19] proposed a stable trapezoidal rule using time step average. The details of the implementation are given, that is, for every n^* step, the following steps are periodically followed to stabilize the integrator.

- 1) Calculate \mathbf{T}_n , $\dot{\mathbf{T}}_n$ and set

$$t_{n+1} = t_n + \frac{1}{2}\Delta t_n. \quad (36)$$

- 2) Update \mathbf{T}_n to the average of \mathbf{T}_n and \mathbf{T}_{n-1}

$$\mathbf{T}_n = \frac{1}{2}(\mathbf{T}_n + \mathbf{T}_{n-1}). \quad (37)$$

- 3) Update the derivative $\dot{\mathbf{T}}_n$ to the average of $\dot{\mathbf{T}}_n$ and $\dot{\mathbf{T}}_{n-1}$

$$\dot{\mathbf{T}}_n = \frac{1}{2}(\dot{\mathbf{T}}_n + \dot{\mathbf{T}}_{n-1}). \quad (38)$$

- 4) Update $\tilde{\mathbf{T}}_n$ by Eq. (29), and update \mathbf{T}_{n+1} and $\dot{\mathbf{T}}_{n+1}$ with the known $\tilde{\mathbf{T}}_n$

$$T_{n+1} = T_n + \frac{1}{4} \Delta t_n \tilde{T}_n, \quad (39)$$

$$\dot{T}_{n+1} = \frac{1}{2} \tilde{T}_n. \quad (40)$$

Then, the next time step is calculated through Eq. (34), and the integral is continued.

Through the average process, the integrator is stabilized, and the adaptive trapezoidal rule without stagnation is realized. In this way, a relatively large time step can be obtained, and the amount of calculation can be effectively reduced.

V. NUMERICAL EXAMPLE

To verify the suitability and effectiveness of the above algorithm in addressing transient heat conduction problems, we use EFG-CN and FEM with CN for comparison. The EFG-CN uses the EFG method for spatial discretization and the fixed-step CN method for time integration. To compare the calculation accuracy, this paper uses L_∞ -norm error, which is defined as

$$\|T^{num} - T^{exr}\|_{L_\infty} = \max_{1 \leq i \leq n} |T_i^{num} - T_i^{exr}|,$$

where T^{num} is numerical solution, T^{exr} is exact solution or reference solution.

Example 5.1. The two-dimensional transient heat conduction problem in a square domain $[0, \pi] \times [0, \pi]$ is considered, and the basic parameters used in the calculation are as follows. The thermal conductivity k , specific heat c_p , and density ρ are taken to be unity. The exact solution is

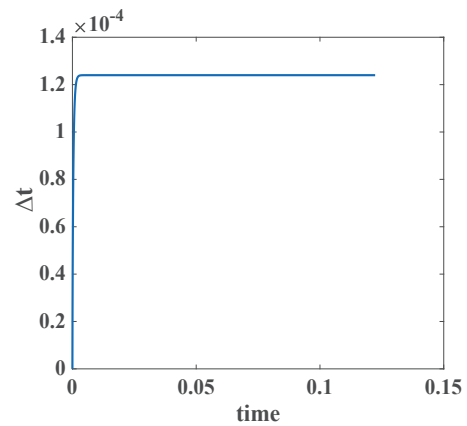
$$T(x, y, t) = e^{-2t} \sin x \cos y.$$

Initial and boundary conditions are capable of being obtained by exact solutions. The time step of EFG-CN method is $\Delta t = 0.01s$.

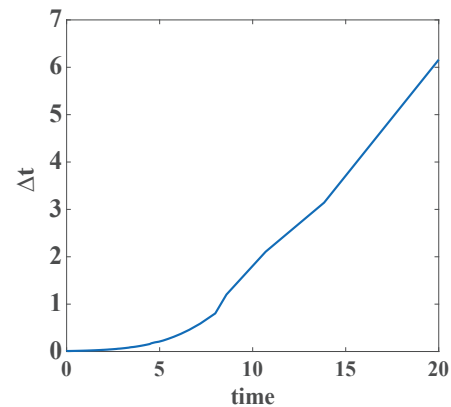
Fig. 1 shows the change of time step obtained by the EFG-TR-AB2 method with time when the average process is not used and the average process is used. It can be seen that without the average process, the ringing effect occurs, and the time step can no longer continue to grow when it is still small. Using the average process, the ringing effect is offset, and the time step can be gradually increased to achieve the desired effect. Therefore, to improve computational efficiency, the average process is a necessary step. The values of n^* in different examples are different. This paper chooses $n^* = 10$.

Fig. 2 shows a comparison between the temperatures obtained using the EFG-TR-AB2 method and the exact solution when $t = 2s$ and the number of nodes is 2601. Fig. 3 shows the temperatures calculated using the EFG-TR-AB2 method and exact solution along $x = \frac{\pi}{2}$ when $t = 2s$ and the number of nodes is 2601. It can be observed from Figs. 2 and 3 that the results calculated using EFG-TR-AB2 method exhibit excellent agreement with the exact solutions, thus verifying the accuracy and feasibility of this proposed method.

Fig. 4 shows the temperatures calculated by EFG-TR-AB2 method and the exact solution at point A $(\frac{\pi}{2}, \frac{\pi}{2})$ changes over time when the number of nodes is 2601. The details in the circle box of Fig. 4 are shown in Fig. 5. It can be observed



(a) The average process is not used to offset stagnation



(b) The average process is used to offset stagnation

Fig. 1. Comparing the time step obtained by the TR-AB2 method without using the average process and using the average process when calculating Example 1.

from Figs. 4 and 5 that the temperatures calculated using EFG-TR-AB2 method is very close to the exact solution. Furthermore, from $t = 0s$ to $t = 20s$, the EFG-TR-AB2 method has only experienced 184 time steps. In contrast, the EFG-CN method needs to experience 2000 time steps because the time step is fixed to 0.01. This indicates that satisfactory accuracy can be achieved using less computational effort by employing the EFG-TR-AB2 method.

Table I shows the calculation time and error of EFG-TR-AB2 and EFG-CN methods when $t = 20s$ under the same node distributions. It is evident from data that as node numbers increase, results from both methods gradually converge while error decreases and calculation time increases. In addition, when compared under the same parameters, both methods have similar levels of accuracy, and the computation time for EFG-TR-AB2 is significantly shorter than that of EFG-CN. In conclusion, when the accuracy requirement is certain, the EFG-TR-AB2 method greatly improves computational efficiency.

Example 5.2. The two-dimensional nonlinear transient heat conduction problem in a square domain $[0, 1] \times [0, 1]$ is considered. Fig. 6 illustrated the geometry and boundary conditions, and basic parameters employed in the calculation are as follows.

The initial temperature $T_0 = 0^\circ C$, the specific heat

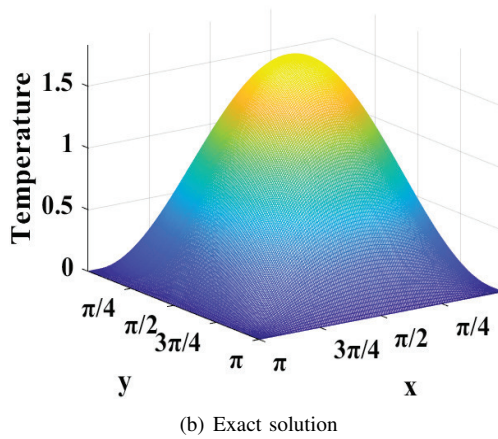
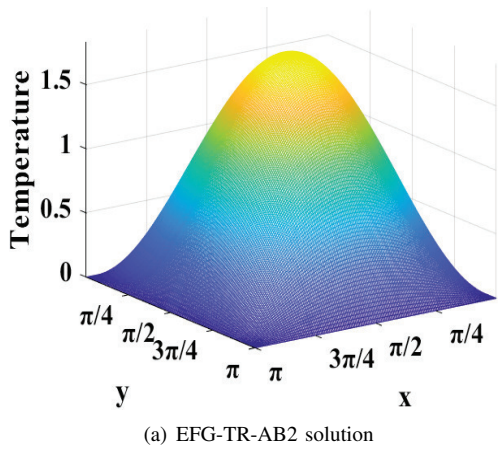


Fig. 2. The comparison between the EFG-TR-AB2 isotherm and the exact solution when $t = 2s$.

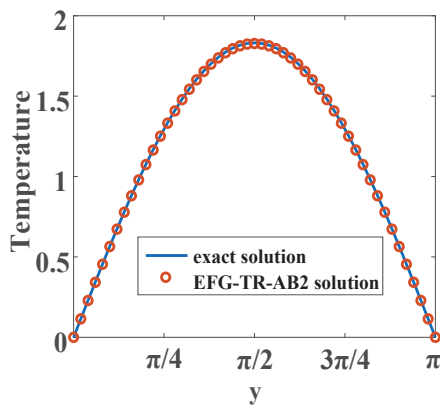


Fig. 3. Comparison of the EFG-TR-AB2 solution along $x = \frac{\pi}{2}$ with the exact solution at $t = 2s$.

TABLE I
THE COMPUTATIONAL TIME AND ERROR OF EFG-TR-AB2 AND EFG-CN WHEN $t = 20s$.

Number of node	error		time	
	EFG-TR-AB2	EFG-CN	EFG-TR-AB2	EFG-CN
2601	0.0029	0.0037	0.3718	7.566
10201	0.0012	0.001	1.937	41.21
22801	6.97E-04	5.22E-04	10.70	127.00
40401	3.09E-04	3.47E-04	43.00	236.00

$c_p = 400 J/kg^\circ C$, the density $\rho = 9000 kg/m^3$, the thermal

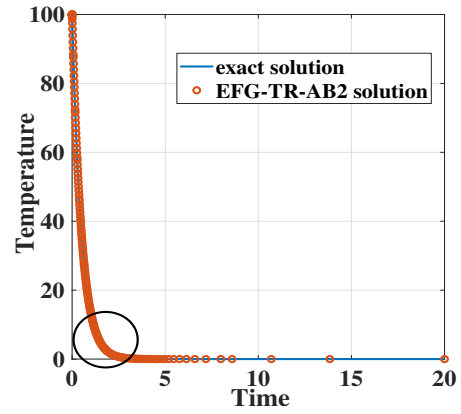


Fig. 4. The temperature distribution of point A ($\frac{\pi}{2}, \frac{\pi}{2}$) with time.

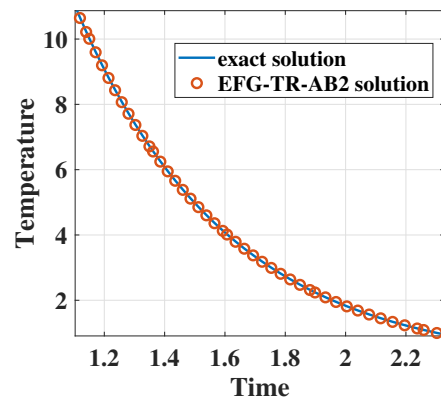


Fig. 5. The detailed results shown in the circle box of Fig. 4.

conductivity $k = 400(1 - \frac{1}{2000}T) W/m^\circ C$. The boundary condition $T = 200^\circ C$ is specified on the left, and the others are $T = 100^\circ C$.

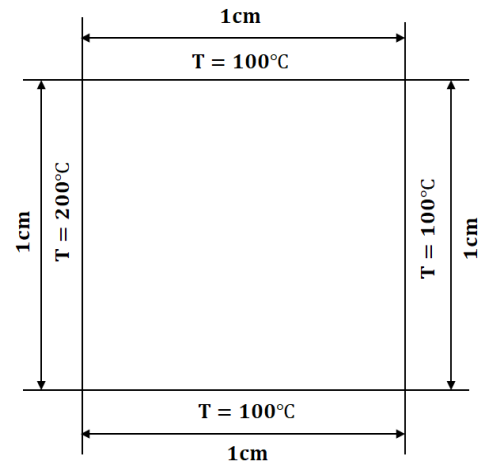


Fig. 6. Geometry and boundary conditions.

EFG-CN method employs the time step $\Delta t = 1s$, and number of nodes is 2601. The time step of the EFG-TR-AB2 method varies with time as shown in Fig. 7. At the end of the figure, a decrease in time step size occurs due to calculation limitations imposed by reaching target times. Fig. 8 shows the isotherms calculated at $t = 1000s$ by the EFG-TR-AB2 method, EFG-CN method, and FEM with 21379 nodes. It

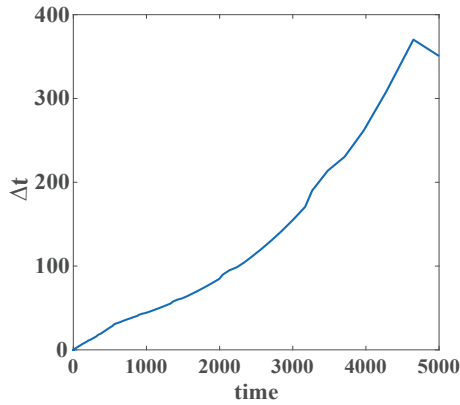


Fig. 7. The time step of TR-AB2 method changes with time.

TABLE II

THE COMPUTATIONAL TIME AND ERROR OF EFG-TR-AB2 AND EFG-CN METHODS ARE CALCULATED WHEN $t = 5000s$.

Number of node	EFG-CN			EFG-TR-AB2	
	Δt	time	error	time	error
2601	1	2.33E+04	0.08		
	5	4.74E+03	0.29	6.71E+02	0.18
	10	2.38E+03	0.67		

is evident that the calculation results of EFG-TR-AB2 and EFG-CN are almost the same as those of FEM with denser meshes, which further proves the stability of our method. Fig. 9(a) illustrates the temperature along $x = \frac{1}{2}$ at $t = 500s$, and Fig. 9(b) illustrates the temperature at point A $(\frac{1}{2}, \frac{1}{2})$ with time. As anticipated, results obtained using the EFG-TR-AB2 scheme closely align with those from EFG-CN methods, thereby validating our proposed approach's accuracy.

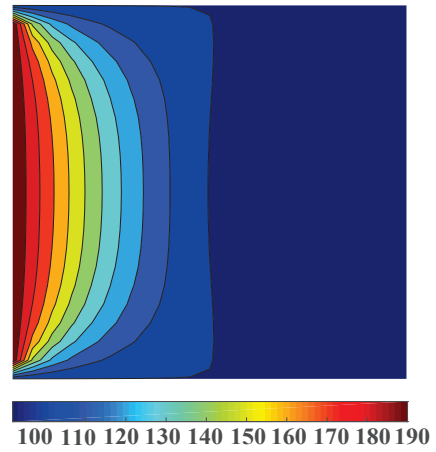
In general, the denser the grid, the higher the accuracy. For comparison, the solution of the EFG-CN method when the number of nodes is 160801 and the time step is $\Delta t = 1s$ is used as the reference solution. Table II shows the calculation time and error of EFG-TR-AB2 and EFG-CN methods when $t = 5000s$. It can be observed that when the error of the two methods is the same order of magnitude, the EFG-TR-AB2 method requires much less calculation time than the EFG-CN method. The obtained numerical results provide additional evidence supporting the effectiveness of the proposed method.

Example 5.3. The two-dimensional transient heat conduction problem in the circular region $\Omega = \{(x, y) | x^2 + y^2 \leq 0\}$ is considered, and the basic parameters used in the calculation are as follows. The thermal conductivity k , specific heat c_p , and density ρ are taken to be unity. The exact solution is

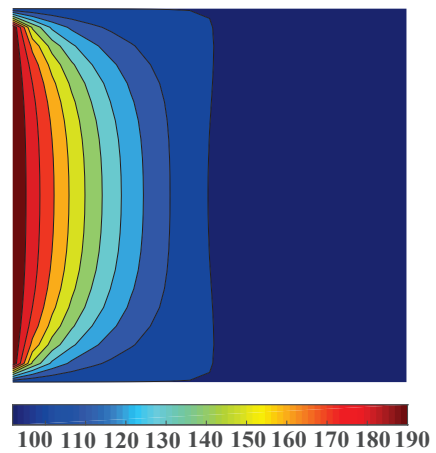
$$T(x, y, t) = 100(e^{-2t} \cos x \sin y + e^{-8t} \cos(2x) \sin(2y)).$$

Boundary condition on the circumference $x^2 + y^2 = 1$ is considered, and the initial condition is capable of being obtained by the exact solution. EFG-CN method employs the time step $\Delta t = 0.01s$, and the number of nodes is 2168. The time step of the EFG-TR-AB2 method varies with time as depicted in Fig. 10.

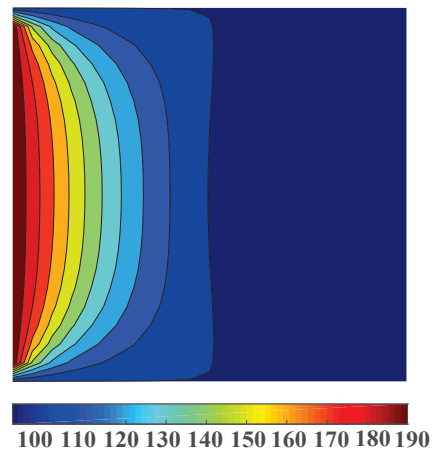
Fig. 11 illustrates the isotherms calculated by the EFG-TR-AB2 method and the exact solution when $t = 1s$. Fig. 11



(a) EFG-TR-AB2 solution



(b) EFG-CN solution

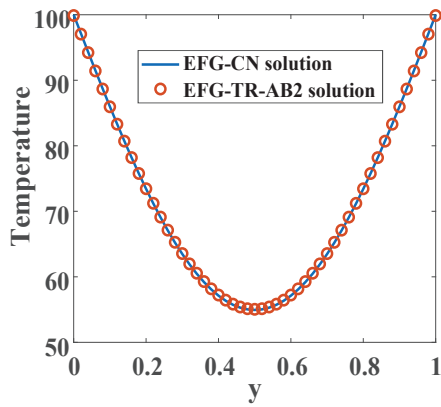


(c) FEM solution

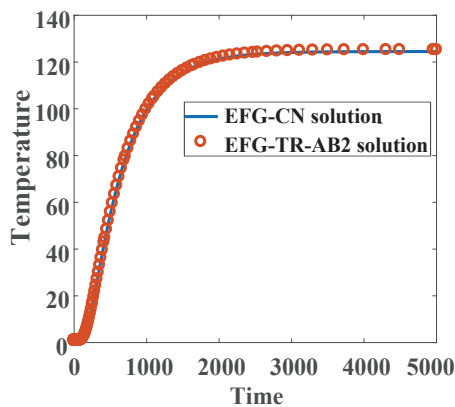
Fig. 8. When $t = 1000s$, the isotherms are calculated using the EFG-TR-AB2 method, EFG-CN method, and FEM respectively.

illustrates excellent agreement between numerical solutions obtained using the EFG-TR-AB2 scheme and exact solutions, thus confirming the reliability of our proposed method for resolving transient heat conduction issues.

Table III shows the calculation time and error of EFG-TR-AB2 and EFG-CN at $t = 20s$. From the data provided by Table III, it is evident that when the error calculated by the EFG-TR-AB2 and EFG-CN methods is in the same



(a) The temperature distribution along $x = \frac{1}{2}$ at $t = 500s$



(b) The temperature distribution of point A $(\frac{1}{2}, \frac{1}{2})$ with time

Fig. 9. Comparison of EFG-CN and EFG-TR-AB2 solutions.

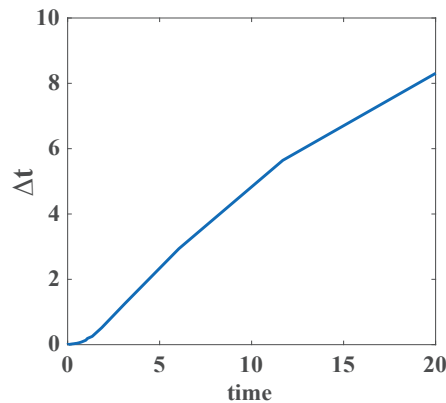
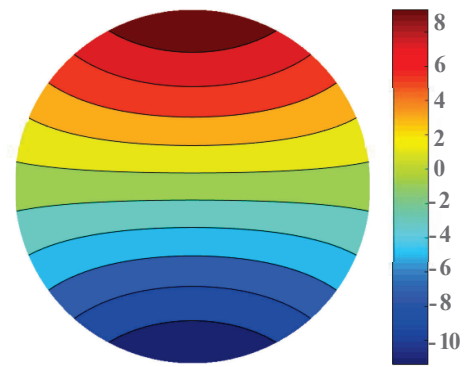


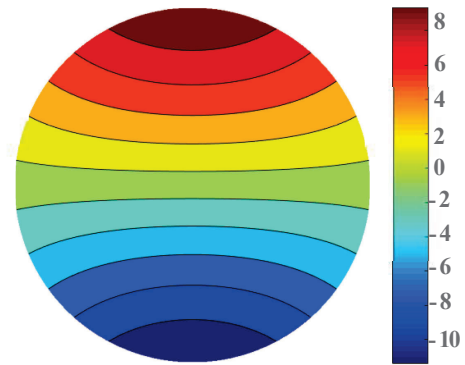
Fig. 10. The time step of TR-AB2 method changes with time.

order of magnitude, the EFG-TR-AB2 method requires less computation time. This further proves that the method given in this paper can obtain satisfactory results for various solution regions, including complex circular regions. Moreover, the EFG-TR-AB2 method demonstrates accurate and stable calculation results, highlighting its potential.

Example 5.4. The fourth example is a heat conduction problem with more complex geometric conditions. Fig. 13 illustrated the geometry and boundary conditions, and the top and bottom edges and hole boundaries are insulated. The



(a) EFG-TR-AB2 solution



(b) Exact solution

Fig. 11. The comparison between the EFG-TR-AB2 isotherm and the exact solution at $t = 1s$.

TABLE III
THE COMPUTATIONAL TIME AND ERROR OF EFG-TR-AB2 AND EFG-CN METHODS ARE CALCULATED WHEN $t = 20s$.

Number of node	EFG-CN			EFG-TR-AB2	
	Δt	time	error	time	error
2168	0.001	57.19	1.69E-04		
	0.01	5.83	0.0016	0.59	0.0028
	0.05	1.16	0.0139		

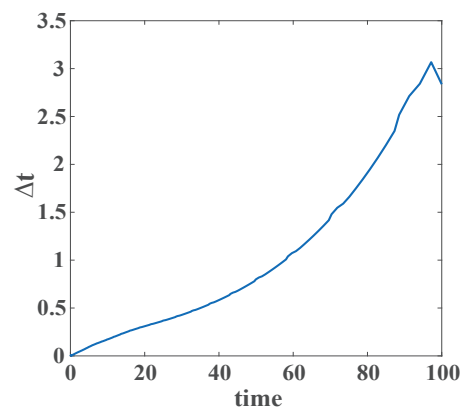


Fig. 12. The time step of TR-AB2 method changes with time.

initial temperature is $T_0 = 1^\circ C$, and the necessary boundary conditions $T = 500^\circ C$ and $T = 20^\circ C$ are specified on the left and right boundaries, respectively. The specific heat $c_p = 200 J/kg^\circ C$, the density $\rho = 5000 kg/m^3$, the thermal conductivity $k = 200 W/m^\circ C$ [22], [34]. EFG-CN method

employs the time step $\Delta t = 0.01s$, and the number of nodes is 4490. The time step of the EFG-TR-AB2 method varies with time as shown in Fig. 12.

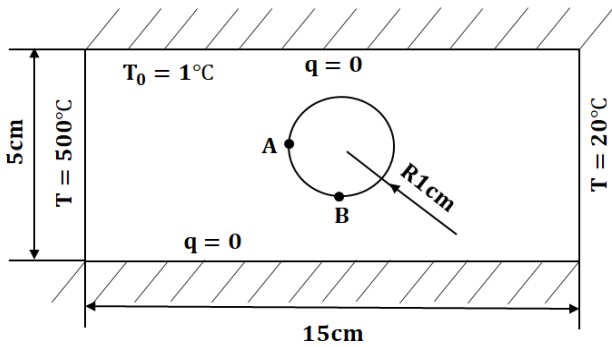
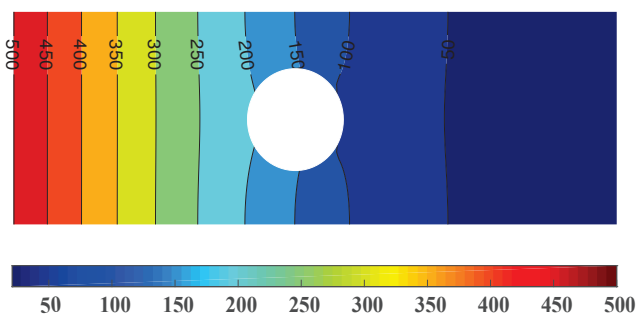
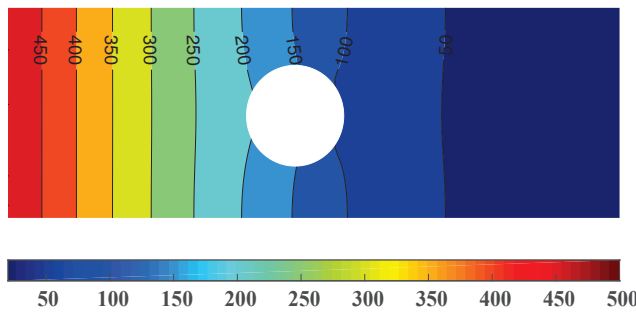


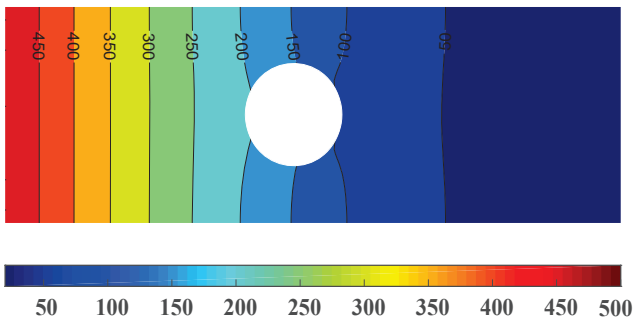
Fig. 13. Geometry and boundary conditions.



(a) EFG-TR-AB2 solution



(b) EFG-CN solution

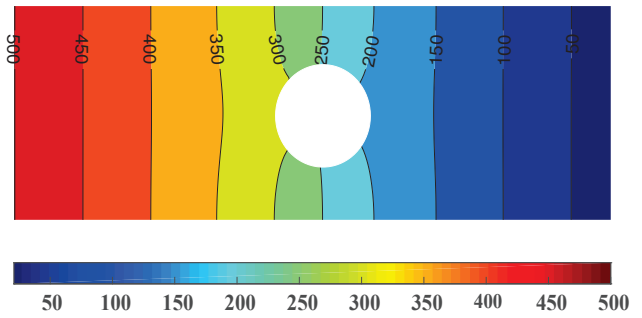


(c) FEM solution

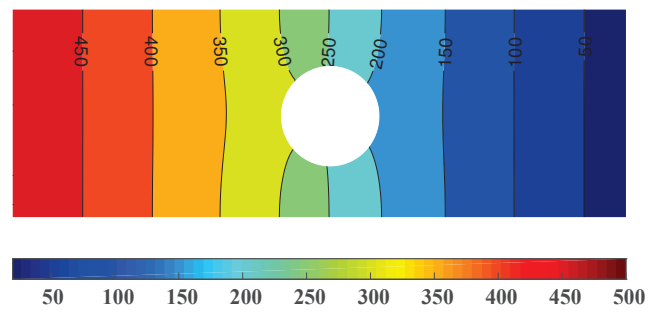
Fig. 14. When $t = 10s$, the isotherms are calculated using the EFG-TR-AB2 method, EFG-CN method, and FEM respectively.

Figs. 14 and 15 illustrate the isotherms calculated at $t = 10s$ and $t = 100s$ by the EFG-TR-AB2 method, EFG-CN method, and FEM with 20410 nodes. From Figs. 14 and 15, it is evident that the results calculated using the EFG-TR-AB2

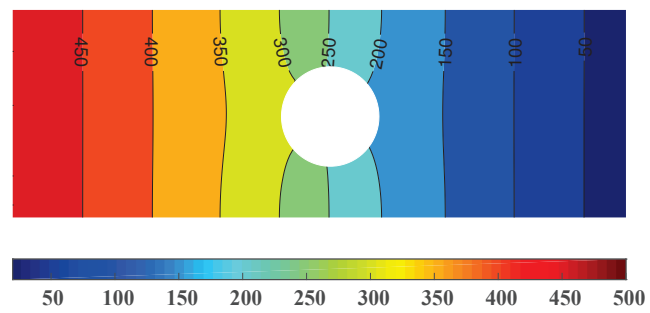
method are almost the same as those of EFG-CN method and FEM with denser meshes. That is to say, the EFG-TR-AB2 method has a good response to the transient heat conduction problem.



(a) EFG-TR-AB2 solution



(b) EFG-CN solution



(c) FEM solution

Fig. 15. When $t = 100s$, the isotherms are calculated using the EFG-TR-AB2 method, EFG-CN method, and FEM respectively.

To quantify the calculation accuracy of the EFG-TR-AB2, Fig. 16 shows the temperature calculation results calculated using the EFG-TR-AB2 method and the EFG-CN method at points A (0.065, 0.025) and B (0.075, 0.015). It is evident that under identical node distributions, the results calculated using EFG-TR-AB2 method and EFG-CN method are very close.

In addition, under the same computer and the same node distribution, the time used for example 4 calculations by the EFG-CN method is 7.108, and the time used for example 4 calculations by the EFG-TR-AB2 method is 1.521, which also shows that the EFG-TR-AB2 method has a very obvious effect in shortening the calculation time compared with EFG-CN method. Numerical results confirm that the EFG-TR-AB2 method applies to transient heat conduction problems, and can effectively enhance the computational efficiency, especially for long-time simulation problems.

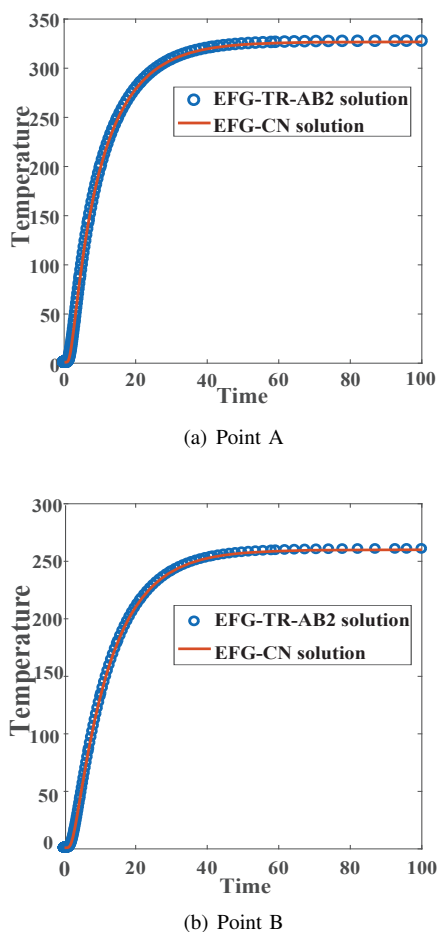


Fig. 16. The temperature at point A (0.065, 0.025) and B (0.075, 0.015) with time.

VI. CONCLUSION

In this work, the EFG-TR-AB2 method is successfully applied to the transient heat conduction problem. EFG-TR-AB2 method employs the EFG method for spatial discretization and the TR-AB2 method for time integration. Compared with the non-adaptive time step, this method significantly reduces the number of time step that need calculation, resulting in substantial savings in wall clock time. Moreover, the adaptive algorithm autonomously determines an optimal time step, omitting the time-consuming simulation experiment to find the appropriate time step. Through several numerical examples, we confirm the accuracy and effectiveness of the EFG-TR-AB2 method obtained by combining the TR-AB2 method with the EFG method. Not only does this approach maintain comparable accuracy to conventional EFG methods but it also considerably shortens prediction times for heat conduction problems, particularly those involving long-term simulations. Furthermore, this method can be easily extended to other meshless methods based on Galerkin weak form, such as meshless local Petrov-Galerkin.

REFERENCES

- [1] T. L. Bergman, A. S. Lavine, F. P. Incropera, and D. P. DeWitt, *Introduction to Heat Transfer*. John Wiley and Sons, 2011.
- [2] R. W. Lewis, P. Nithiarasu, and K. N. Seetharamu, *Fundamentals of the Finite Element Method for Heat and Fluid Flow*. John Wiley and Sons, 2004.
- [3] B. Yu, H. L. Zhou, H. L. Chen, and Y. Tong, "Precise time-domain expanding dual reciprocity boundary element method for solving transient heat conduction problems," *International Journal of Heat and Mass Transfer*, vol. 91, pp. 110–118, 2015.
- [4] Q. Li, S. Chen, and X. Luo, "Steady heat conduction analyses using an interpolating element-free Galerkin scaled boundary method," *Applied Mathematics and Computation*, vol. 300, pp. 103–115, 2017.
- [5] X. Cao, X. Zhang, and X. Shi, "An adaptive variational multiscale element free Galerkin method based on the residual-based a posteriori error estimators for convection-diffusion-reaction problems," *Engineering Analysis with Boundary Elements*, vol. 136, pp. 238–251, 2022.
- [6] X. Zhang, K. Z. Song, M. W. Lu, and X. Liu, "Meshless methods based on collocation with radial basis functions," *Computational Mechanics*, vol. 26, pp. 333–343, 2000.
- [7] H. Y. Hu, J. S. Chen, and W. Hu, "Error analysis of collocation method based on reproducing kernel approximation," *Numerical Methods for Partial Differential Equations*, vol. 27, no. 3, pp. 554–580, 2011.
- [8] T. Belytschko, Y. Y. Lu, and L. Gu, "Element-free Galerkin methods," *International Journal for Numerical Methods in Engineering*, vol. 37, no. 2, pp. 229–256, 1994.
- [9] W. K. Liu, S. Jun, and Y. F. Zhang, "Reproducing kernel particle methods," *International Journal for Numerical Methods in Fluids*, vol. 20, no. 8-9, pp. 1081–1106, 1995.
- [10] A. Singh, I. V. Singh, and R. Prakash, "Meshless element free Galerkin method for unsteady nonlinear heat transfer problems," *International Journal of Heat and Mass Transfer*, vol. 50, no. 5-6, pp. 1212–1219, 2007.
- [11] R. Sharma, "Effect of viscous dissipation and heat source on unsteady boundary layer flow and heat transfer past a stretching surface embedded in a porous medium using element free Galerkin method," *Applied Mathematics and Computation*, vol. 219, no. 3, pp. 976–987, 2012.
- [12] H. Cheng, M. Peng, and Y. Cheng, "A hybrid improved complex variable element-free Galerkin method for three-dimensional advection-diffusion problems," *Engineering Analysis with Boundary Elements*, vol. 97, pp. 39–54, 2018.
- [13] X. Zhang, P. Zhang, and L. Zhang, "An improved meshless method with almost interpolation property for isotropic heat conduction problems," *Engineering Analysis with Boundary Elements*, vol. 37, no. 5, pp. 850–859, 2013.
- [14] F. Sun, J. Wang, and Y. Cheng, "An improved interpolating element-free Galerkin method for elastoplasticity via nonsingular weight functions," *International Journal of Applied Mechanics*, vol. 8, no. 08, p. 1650096, 2016.
- [15] J. F. Wang, F. X. Sun, and Y. M. Cheng, "An improved interpolating element-free Galerkin method with a nonsingular weight function for two-dimensional potential problems," *Chinese Physics B*, vol. 21, no. 9, p. 090204, 2012.
- [16] F. Sun, J. Wang, Y. Cheng, and A. Huang, "Error estimates for the interpolating moving least-squares method in n-dimensional space," *Applied Numerical Mathematics*, vol. 98, pp. 79–105, 2015.
- [17] F. Sun, J. Wang, Y. Wu, and Q. Wei, "An improved element-free Galerkin method based on the dimension splitting moving least-squares method for 2D potential problems in irregular domains," *International Journal of Applied Mechanics*, vol. 14, no. 10, p. 2250065, 2022.
- [18] J. De Frutos, B. García Archilla, and J. Novo, "An adaptive finite element method for evolutionary convection dominated problems," *Computer Methods in Applied Mechanics and Engineering*, vol. 200, no. 49-52, pp. 3601–3612, 2011.
- [19] P. M. Gresho, D. F. Griffiths, and D. J. Silvester, "Adaptive time-stepping for incompressible flow part I: Scalar advection-diffusion," *SIMA Journal on Scientific Computing*, vol. 30, no. 4, pp. 2018–2054, 2008.
- [20] M. Mayr, W. Wall, and M. Gee, "Adaptive time stepping for fluid-structure interaction solvers," *Finite Elements in Analysis and Design*, vol. 141, pp. 55–69, 2018.
- [21] M. Mortezaadeh and L. Wang, "An adaptive time-stepping semi-lagrangian method for incompressible flows," *Numerical Heat Transfer, Part B: Fundamentals*, vol. 75, no. 1, pp. 1–18, 2019.
- [22] X. Zhang and H. Xiang, "A fast meshless method based on proper orthogonal decomposition for the transient heat conduction problems," *International Journal of Heat and Mass Transfer*, vol. 84, pp. 729–739, 2015.
- [23] N. Young, *An Introduction to Hilbert Space*. Cambridge University Press, 1988.
- [24] D. Mirzaei, "Analysis of moving least squares approximation revisited," *Journal of Computational and Applied Mathematics*, vol. 282, pp. 237–250, 2015.

- [25] Z. Ullah and C. Augarde, "Finite deformation elasto-plastic modelling using an adaptive meshless method," *Computers and Structures*, vol. 118, pp. 39–52, 2013.
- [26] D. P. Bertsekas, *Constrained Optimization and Lagrange Multiplier methods*. Academic Press, 2014.
- [27] N. I. M. Gould, "On the convergence of a sequential penalty function method for constrained minimization," *SIAM Journal on Numerical Analysis*, vol. 26, no. 1, pp. 107–128, 1989.
- [28] L. Zhang, J. Ouyang, and X. Zhang, "The variational multiscale element free Galerkin method for MHD flows at high Hartmann numbers," *Computer Physics Communications*, vol. 184, no. 4, pp. 1106–1118, 2013.
- [29] G. R. Liu and Y. T. Gu, *An Introduction to Meshfree Methods and Their Programming*. Springer Science and Business Media, 2005.
- [30] G. K. Prinja, "Adaptive solvers for elliptic and parabolic partial differential equations," Ph.D. dissertation, Manchester Institute for Mathematical Sciences, The University of Manchester, 2010.
- [31] J. A. Lee, J. Nam, and M. Pasquali, "A new stabilization of adaptive step trapezoid rule based on finite difference interrupts," *SIMA Journal on Scientific Computing*, vol. 37, no. 2, pp. A725–A746, 2015.
- [32] G. G. Dahlquist, "A special stability problem for linear multistep methods," *BIT Numerical Mathematics*, vol. 3, no. 1, pp. 27–43, 1963.
- [33] P. Gresho, R. Lee, R. Sani, C. Taylor, and K. Morgan, "Recent advances in numerical methods in fluids," *Pineridge Swansea*, pp. 27–79, 1980.
- [34] K. Yang and X. W. Gao, "Radial integration BEM for transient heat conduction problems," *Engineering Analysis with Boundary Elements*, vol. 34, no. 6, pp. 557–563, 2010.